Analysis and Improvement of CT-Scan/MRI Medical Image Quality in Stroke Patients with Hybrid Thresholding Method: A Case Study in Padang BMC Hospital

Sumijan [a,*], Pradani Ayu Widya Purnama [a]

[a] Faculty of Computer Science, Universitas Putra Indonesia YPTK Padang, Lubuk Begalung Highway, Padang, 25000, Indonesia
*Corresponding author: *sumijan@upiyptk.ac.id*

Abstract— **Stroke as one of the main problems in the medical field. From the three leading causes of death in the world including 13% are coronary heart disease and 12% are cancer. Stroke occurs mostly in developed countries such as Indonesia, of all deaths in Indonesia, the cause of stroke is 7.9%. One of the efforts to minimize the risk of stroke is take preventive measures in stroke patients, before and after an attack. Ways to overcome stroke are primary and secondary measures. Prevention of stroke symptoms can be avoided by prompt and appropriate treatment in stroke care according to medical service standards. This study applies texture analysis and improves the quality of CT-Scan or MRI brain images using the Hybrid Thresholding (HT) method, which combines edge detection and P-File methods. Differences the texture of the image a brain hemorrhage that is indicated by stroke and clarify the quality of the image of a brain hemorrhage that is indicated by a stroke with the parameters of contrast, correlation, energy, homogeneity. The results of segmentation and feature and texture extraction are then classified using the Backpropagation Neural Network (BNN) method with variations in the learning rate value, resulting in the best test at a learning rate of 0.1 with an error percentage of 2%. The results of the classification of the calculation of the area of brain bleeding and analysis of image quality in classifying brain strokes with an accuracy level are: 27 / 3 x 100% = 90.0%.**

Keywords— **CT-Scan/MRI; Brain hemorrhage, stroke, Texture analysis, Hybrid thresholding method.**

I. INTRODUCTION

According to the World Stroke Organization (WSO), stroke has contributed to mortality, and the risk of disability is very high. From the WSO data, the risk of physical disability from the cause of stroke can occur in the productive age and the elderly. In some hospitals, the mortality rate due to stroke reaches 20% within 28 days of hospitalization. Out of six people, one person has had a stroke during their lifetime [1]. The results of research from the American Health Association (AHA) show that every 40 minutes, there is one new case of stroke, both new and recurrent, reaching 795,000 patients, and it is predicted that every 4 minutes, there is one stroke patient who dies. The cause of death due to stroke in the United States has reached 1 in 20 patients died from stroke [2]. Data from the World Health Organization (WHO) shows that one of the causes of death in Indonesia is stroke, which is 7.9% of all deaths [3]. The percentage of stroke in Indonesia from the diagnosis of health workers is 7 per 1000 Indonesian population diagnosed with stroke symptoms is 12.1 per 1000 population. Stroke based on the results of Ministry of Health of the Republic of Indonesia report in 2018 [41] that the highest percentage is in South Sulawesi at 17.9%, then Yogyakarta Special Region at 16.9%, followed by Southeast Sulawesi at 16.6%, then East Java at 16% [4]. The highest percentage of strokes in South Sulawesi was 17.9%, where the largest stroke occurred at the age of over 75 years at 84.6% and men at 17.3% [5].

The technique of imaging the pathological type of stroke uses neuroimaging Computerized Tomography (CT) Scan of the head or with Magnetic resonance imaging (MRI). The performance of CT scans in depicting new stroke pathology images will appear after one day [6], [7], [8]. MRI is an alternative to speed up the imaging technique of stroke pathology, which has a high resolution compared to CT scans, but MRI still has weaknesses because if the depiction is not a stroke, then a medical person still considers it a minor stroke,

this can cause errors in the image take a medical decision because it cannot be detected by either CT scan or MRI [9].

Image processing can provide solutions to diagnose stroke in detail and perform analysis ranging from quality improvement to segmentation, extraction, and identification. As an input image, it can be done using a CT scan or MRI where the stroke will be known as a dark area (hypodense) with contrast relative to the surrounding area, for a very small one with a dim intensity that cannot be detected by a CT scan or MRI [10],[11]. To overcome the dim intensity that a CT scan or MRI cannot detect, it is necessary to use the right methods and techniques so that the results of calculating the volume of the bleeding area are valid. Therefore, it is necessary to do segmentation for precision, which means more selective in doing ROI (Region Of Interest), so the bleeding area can be seen clearly. The areas that are not bleeding areas are not included in the ROI [12]. Circulating cerebral hemorrhage micro embolism in a hospitalized patient who is positive for COVID-19 and has had an unexplained stroke. For brain hemorrhage, microemboli and positive for COVID-19 require further medical investigation [13], [14]. The automatic segmentation method can be done by depicting the bleeding stroke through CT Scan or MRI. Some studies only discuss the problems encountered in segmenting CT scans and MRI images and the relative benefits and limitations of currently available methods for segmenting medical images [15], [16], [17]. Deep learning-based medical image segmentation is still experiencing difficulties in several studies. The level of segmentation accuracy is not high, the number of medical images in the image collection file is small, and the intensity and resolution are very low. Inaccurate segmentation results cannot meet the clinical requirements medically expected by the medical party [18], [19]. This study improves the quality and analyzes CT-Scan/MRI Medical Images on images of brain stroke patients with the hybrid thresholding method to provide recommendations to the medical community regarding the level of clarity, area, and volume of the brain stroke area. This study also classifies the results of the calculation of the area and volume of the area of brain stroke to analyze the type of stroke. Thus, this study provides recommendations for further medical action.

II. Material and Method

A. Stroke Brain Blending

The brain is a very soft and tender organ of the body that consists of several parts. The largest part is dominated by the cerebrum, which controls speech, memory, and emotions. The brain is very susceptible to damage and bleeding. In principle, the brain has very good protection because the brain has been protected in various layers. Outside the brain is also protected by the skull of several types of interconnected bones. However, many factors can cause bleeding in the brain and surrounding area. In bleeding that cannot be controlled can cause brain cell death and the cessation of many functions in the body that can be controlled.

Uncontrolled bleeding can cause temporary or permanent brain function death and result in motor skill loss. There are four types of bleeding in the brain, namely: Stroke is categorized into clinical syndromes to determine the type of stroke that has been described using a CT scan or MRI (imaging) can be distinguished based on: vascular or non-vascular (tumor or infection) (2). Ischemic (bleeding stroke), (3). arterial or venous infarcts, (4). anterior or posterior circulation stroke will be used to determine whether carotid stenosis is symptomatic or not [20], [21], as shown in figure 1.

Imaging technology that is developing rapidly, such as CT scans or MRI, can describe which tissue can be saved in stroke patients before receiving intensive care and treatment. However, a CT scan or MRI can describe stroke patients, whether infarction or bleeding, which takes five days after the stroke patient's acquisition. To distinguish a hemorrhagic stroke or not an ordinary hemorrhagic stroke, it is determined by high intensity (in white color) and round shape attached to the infarct area. Usually, low intensity (in dark color) occupies several areas of swelling, as shown in Figure 1 [22],[23].
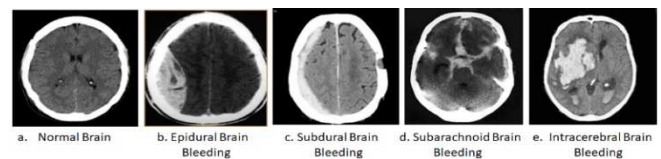

Fig. 1 Normal Brain CT Scan Results and Bleeding

In patients with stroke indications who have been acquired using a CT scan, usually, normal patients do not experience bleeding; the medical community considers this an infarct. If sharpening is done for the contrasting interval, it is not necessary because the diagnosis will be ambiguous. Small hemorrhages sometimes cannot be detected at what high intensity (white) should be, so they do not appear low intensity compared to normal brain. This gives different information about infarction or not. For ten days, minor bleeding will not be able to distinguish between infarction and minor bleeding because, in 7 days, it disappears. Moderate Heavy bleeding persists for 2 to 3 weeks. Optimization is needed to speed up the time in describing stroke patients. CT scan or MRI can describe the image of stroke patients to get the results of the patient's diagnosis, whether including infarction or not. Because the CT scan results indicated an infarct did not become hypodense, it could take hours or even one day after the stroke was indicated [24],[25].

B. Digital Images

Image is one element that represents an object. Image consists of 2 categories, namely analog images and digital images, analog images depict objects continuously such as satellite images, television monitor images, x-ray photos while digital images from CT scan photos, MRI, digital cameras that can be processed by computer [26], [27]. Digital images are described in the form of a matrix consisting of M columns and N rows, from the M, N or x, y coordinates as pixels or called picture elements, pixels are the smallest elements of digital image elements. A pixel has two variables: the coordinates (location / place) where the pixel is located and the intensity or color of the pixel. The intensity value is assumed to be f and the coordinates are assumed to be (x,y) so that the value of a pixel is defined as a function f(x,y). Digital images consist of 2 dimensions and can be visualized on a computer monitor screen (video graphics adapter) which is a finite (discrete) set of digital values called picture elements [28].

C. Contrast Stretching

Contrast can be caused by light conditions that are not regularly distributed on the object part or the influence of the limited number of sensors in recording illumination events. Figure 2 shows a typical transformation used in the contrast stretching process, where the value scale is between 0 to 255, and the image is assumed to have a grayscale.
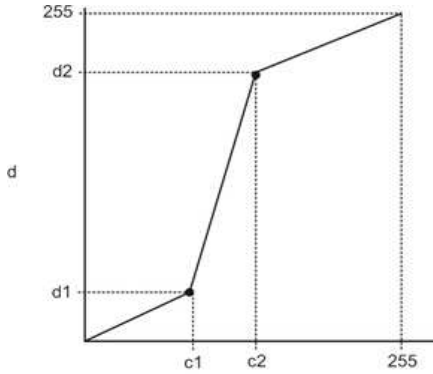

Fig. 2 Contrast Stretching Typical Transformation Results

In Figure 2, two points are depicted: points (c1, d1) and points (c2, d2), which are used to determine the pattern as a transformation function. The purpose of the transformation is to determine the distribution of grayscale intensity in the assumed image. If c1 = c2 and d1 = d2, then a straight-line transformation is formed, meaning that there is no change in the gray intensity of the resulting image. If c1<=c2 and d1<=d2, a single value transformation is formed where the value will always increase.

D. Threshold Method

This method is used to determine the threshold value; the input of the process of finding the threshold value is a gray image, then converted to a binary image to obtain the optimal threshold value. Thresholding can be local and global depending on the characteristics of the image to be processed. Thresholding is defined as a segmentation method of digital image processing to separate objects and backgrounds from an image, where the image can be distinguished by determining the brightness or dark intensity of the image to be segmented. The dark intensity area of the image is 0, and the light intensity area is 1 [29]. The output of the segmentation process using the thresholding method produces a binary image with a pixel intensity value of 0 or 1. The formula used in the thresholding method uses equation (1), as follows:

$$g(X,Y) = \begin{cases} 1 \; F(X,Y) < T \\ 0, f(x,y) \geq T \end{cases} \qquad (1)$$

E. Hybrid Thresholding Method (HT)

The Hybrid Thresholding method, abbreviated as HT, is used to determine the threshold value faster than the OTSU method developed by Samopa and Asano [30]. The working principle of the HT method by combining the P-File method and the commonly used edge detection methods such as Canny, Sobel, Prewitt, Robert, and LoG [31], the HT method produces a segmentation process that is faster and has a high level of accuracy compared to the HT method. OTSU. In the HT method, the value of image I becomes the original image, and G, the result of the HT method process, becomes a new

threshold value which will be carried out by the process of searching for the optimal threshold value [32] the algorithm of the HT method is as follows :

```
1. O ← EdgeMap(I)  # Compute EdgeMap from I image #
2. v ← initial Value
3. e ← RealMax # et e as the maximum image value #
4. Loop until v = max_Value in Step increment.
5. T ← P-tile(I,v)  # threshold I using P-tile method and v as
   threshold value #
6. C ← EdgeMap(T) # Calculate Edge Map of T . image #
7. r ← MSE(O,C)   # Calculate MSE value in O and C #
8. If  r < e  # if the MSE value is less than e #
9. e ← r # exchange the value of e with the value of MSE#
10. G ← v # set v as lookup value #
```

The HT method is very simple in the segmentation process; it is adjusted to the type and characteristics of the image to be processed to find the optimal threshold value. The iteration process is carried out continuously until it gets the most optimal value. This HT method combines the P-File method and the existing edge detection method, where the process carried out will determine the best edge detection value commonly used, such as Canny, Sobel, Prewitt, Robert, and LoG [33].

F. Principal Component Analysis (PCA)

Principal Component Analysis is a multivariate analysis that transforms original correlated variables into new, uncorrelated variables by reducing the number of these variables so that they have smaller dimensions but can explain most of the diversity of the original variables. The number of principal components formed equals the number of original variables. [34]. The results of Yang et al [42] carried out a lot of data extraction and produced a data structure with a new and very good pattern and produced quite a lot of dimensions, where the extraction results found the right eigenvalues and eigenvectors with an accuracy rate of 98% [35]. In the process of perpendicular transformation in the coordinates to describe the data. The choice of coordinates must determine the variance that reaches the maximum value. Figure 3 shows how the PCA algorithm works, where PCA projects an image in its eigenspace using a technique by finding the eigenvectors of each image and projecting it into the eigenspace obtained. The magnitude value of the eigenspace is determined based on the number of training images used [36], as illustrated in Figure 3.
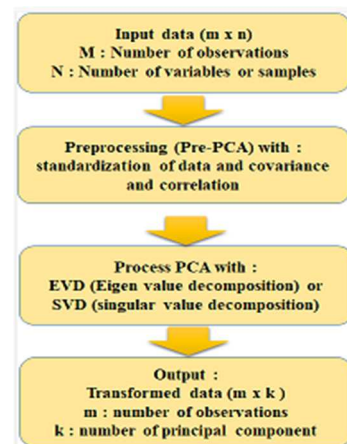

Fig. 3 Principal Components Analysis Steps

G. Backpropagation Neural Network (BNN)

A backpropagation neural network (BNN) is needed to balance the network's performance in order to recognize patterns. BNN is used to provide a valid response from the input pattern with a similar (but not the same) level as the pattern used during the training. BNN has multiple layers contained in hidden neuron units. BNN architecture with n inputs plus 1 bias and m output units. Figure 4 shows the BNN architecture, where V_{ij} is the line weight from the input unit Xi to the hidden layer unit Zj(Vj0), a line connecting the bias in the input unit to the hidden layer unit Zj). While Wkj is the weight of the hidden layer unit Zj to the output unit Yk (Wk0 is the weight of the hidden layer bias to the output unit (Yk). The BNN architecture is shown in Figure 4. [36],[37],[38].
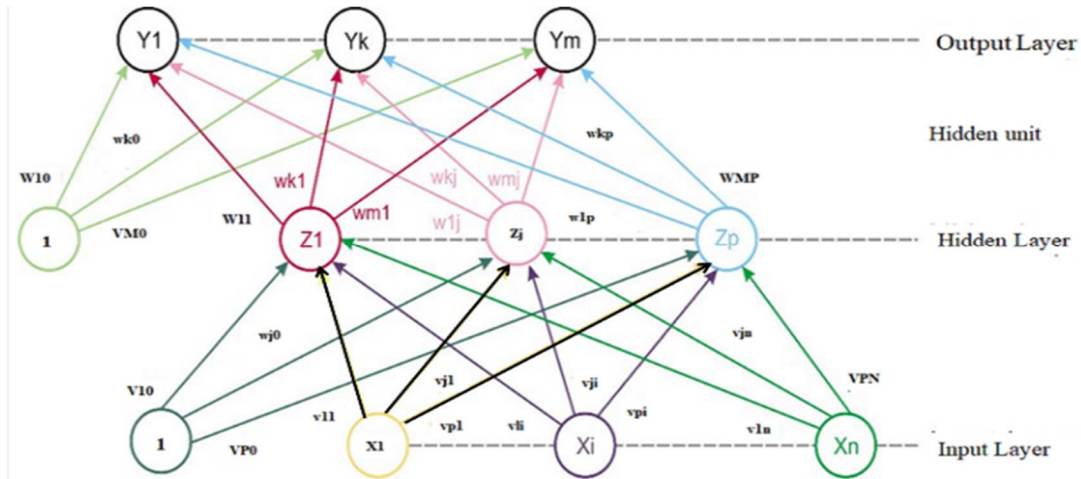
Fig. 4 BNN General Architecture with one hidden layer.

The explanation of Figure 4 is as follows:
1. BNN can have more than 1 input layer in one or more hidden layers. The BNN architecture has an input layer and a bias layer, a hidden layer consisting of p units plus 1 bias layer and m unit output layers.
2. V_{ij} is the weight of the axis line from the input unit Xi to the hidden layer unit Zj, where Vj0 is the weight of the axis line connecting the bias layer in the input unit to the hidden layer unit Zj. W_{kj} as the weight of the hidden layer unit Zj to the output unit Y_k, where Wk0 as the weight of the bias layer on the hidden layer to the output unit Y_k.

The BNN algorithm was first introduced by Werbos and popularized by Rumelhart and Mc. Clelland. BNN is a mathematical calculation technique with a formula that determines each layer. BNN is a type of artificial neural network (ANN) using the supervised learning method (supervised learning) [39], [40]. In supervised learning, there is a pair of input and output data that is used to train the artificial neural network until the desired weight is obtained. Weathers function as a liaison between layers in an artificial neural network. The BNN algorithm has a training process step that is based on a simple interconnection, i.e., If the output still gives incorrect results, then the weights are corrected so that the error value can be minimized, and the response from the artificial neural network is then expected to approach the valid value. The steps carried out in the BNN algorithm are described as follows:
1. The initial value of the weight of the smallest random value is between 0 to 1.
2. A pair of vectors is trained to start from steps 3 to 8.
3. Each input unit (Xi where i=1,2,3...,n) receives input from Xi and performs the input process to all units in the layer above it or further as a hidden layer.
4. Each hidden unit Zj, where j=1,2,3,..,p) adds up its weight with each input value using the equation:

$$Z_{netj} = v + \sum_{i=1}^{n}(xiyij) \qquad (2)$$

then use the activation function to calculate the output value using the following equation:

$$Z = f(Z_{netj}) \qquad (3)$$

then sent to the input to all the upper layer units on the output layer units.
5. Each output Yk, where k=1,2,3,..,m) the total weight of each uses the following equation:

$$Y_{netk} = W_{ok} + \sum_{i=1}^{p}(ZiWk) \qquad (4)$$

Furthermore, by using the activation function to calculate the output value using the equation:

$$y_k = f(Y_{netk}) \qquad (5)$$

then sent to the input to all the units of the layer above it on the output layer units.
6. Each Yk output, where k=1,2,3,..,m) is given a target pattern that is connected using a learning input pattern, to calculate the error value using the following equation:

$$\sigma_k = (t_k - y_k)f'(y_{netk}) = (t_k - y_k)\, y_k\,(1 - y_k) \qquad (6)$$

Next, calculate the weight correction to be used in improving the Wjk value, using the following equation:

$$\nabla W_{jk} = \sigma * \vartheta * Z_j \qquad (7)$$

Also calculate the bias correction that will be used to correct the W0k value, then send it to the layer units below it, using the equation:.

$$\nabla W_{jk} = \sigma\vartheta_k \qquad (8)$$

7. Each hidden unit Zj, where j=1,2,3,..,p) adds up the input delta of the units in the layer above it, using the following equation:

$$\delta_{netj} = \sum_{k=1}^{m}(\delta_k W_{jk}) \qquad (9)$$

multiply the value by the derivative of the activation function to calculate the error information, using the equation:

$$\delta_j = \delta_{netj} * f'\left(Z_{netj}\right) = \delta_{netj} Z_j \left(1 - Z_j\right) \qquad (10)$$

then calculate the weight correction that will be used to improve the value of Vij, using the equation:

$$\nabla v_{jk} = \sigma * \delta_j X_i \qquad (11)$$

calculate the bias correction that will be used to correct the value of V0j, using the equation:

$$\Delta v_{ok} = \sigma * \delta_j \qquad (12)$$

8. Each output unit Yk, where k=1,2,3,..,m) to correct the bias value and weight value, use the equation:

$$W_{jk}\left(baru\right) = W_{jk}\left(lama\right) + \Delta v_{ok} \qquad (13)$$

each hidden unit Zj where j=1,2,3,..,p) corrects the bias and weights, where i=0,1,2,..,n), using the equation:

$$v_{ij}\left(baru\right) = v_{ij}\left(lama\right) + \Delta v_{ij} \qquad (14)$$

9. End of test conditions.
   Stages 3 to 5 are part of a feed-forward, and stages 6 to 8 are part of backpropagation.

H. Related Works

In this study, analysis, and improvement of the image quality of brain bleeding in Epidural, Intracerebral, Subarachnoid, and Subdural stroke patients will be carried out from the CT-Scan results using the HT method. The research stages include literature study, system design, testing and evaluation, scientific paper publication, dissertation completion, and book publication. These stages can be seen in Figure 5.
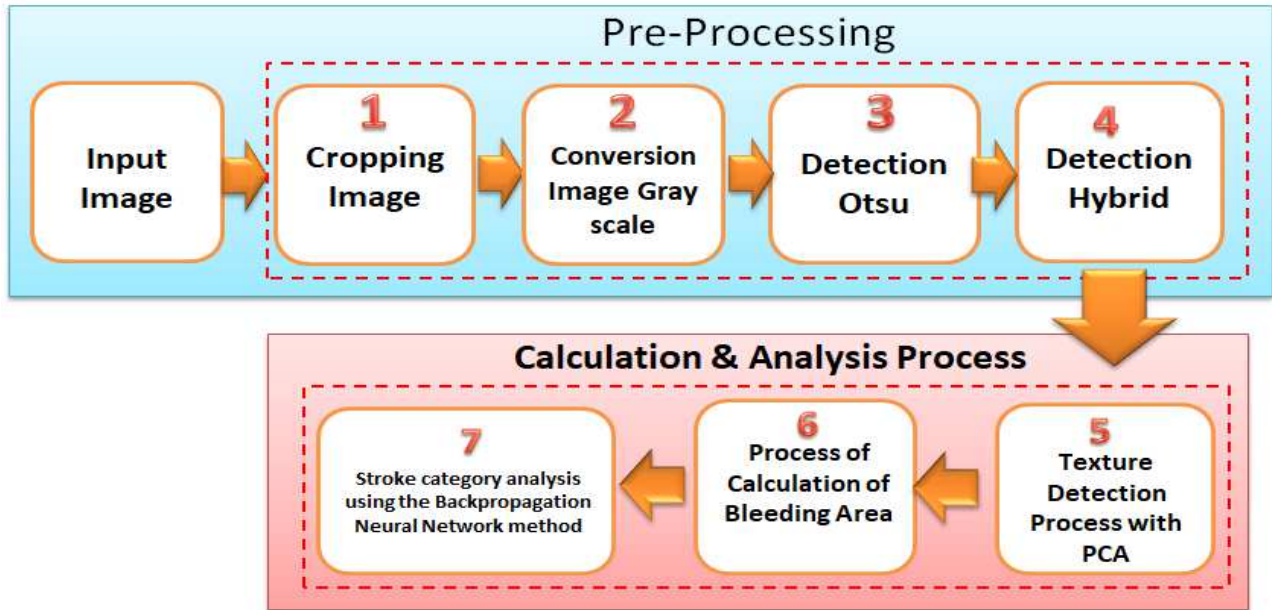
Fig. 5 Research framework

1. Input images from CT scan/MRI taken from Padang City BMC Hospital will be stored in a jpg database.
2. 16-bit image to be recognized as RGB, to simplify the process, it is necessary to change the intensity from RGB to gray level, and an algorithm is needed to recognize bleeding brain images and normal ones.
3. Separating the object and the background to detect and determine the bleeding in the brain so that bleeding and non-bleeding can be separated using the Otsu method.
4. The segmentation process is carried out to obtain a separation between 1 or more bleeding to determine how much bleeding occurs in the brain using the hybrid thresholding method.
5. The area of bleeding is determined using the PCA method to identify the bleeding pattern in detail so that it can be analyzed.
6. To calculate the area of bleeding using an algorithm to calculate the area of bleeding detected in white in the previous process so that the number of pixels of white intensity in the area of brain bleeding is obtained.

7. Analyze and classify brain bleeding related to the type of stroke using the BNN method, whether it includes Epidural, Intracerebral, Subarachnoid, Subdural, or normal strokes.

III. RESULTS AND DISCUSSION

Measurement of brain bleeding volume of patients with intracerebral hemorrhagic stroke results is from MSCT. It begins with retrieving image data from CT scan, computer processing volume viewer, determining the target value for bleeding volume from radiologists 1 and 2, and bleeding volume results from GVF snake results. The results of all patients measuring bleeding volume from the Radiology Laboratory of Bunda Medical Center Hospital (RS. BMC) Padang City can be seen in Table I. The results of improving the image quality of Brain Bleeding and Normal Brain Edge Detection results with the Hybrid Thresholding method can be seen in Table II.

TABLE I

THE RESULTS OF ALL PATIENTS MEASURING THE VOLUME OF BLEEDING FROM THE RADIOLOGY LABORATORY OF BUNDA MEDICAL CENTER HOSPITAL (RS. BMC) PADANG CITY
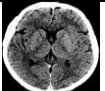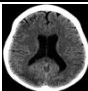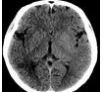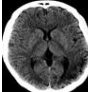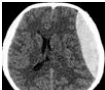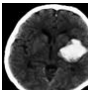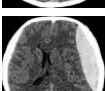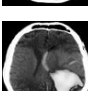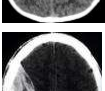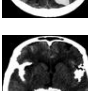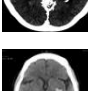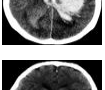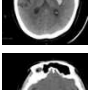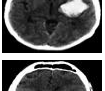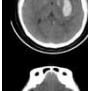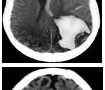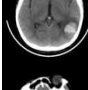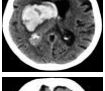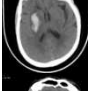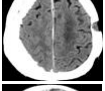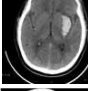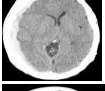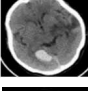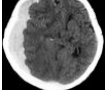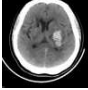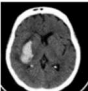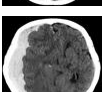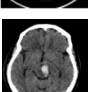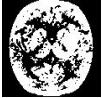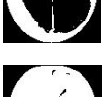
No	Patient Code	Original Image	No	stroke category	Patient Code	Original Image	stroke category
1.	P-01		16	Normal	P-16		Subarachnoid
2.	P-02		17	Normal	P-17		Normal
3.	P-03		18	Epidural	P-18		Normal
4.	P-04		19	Epidural	P-19		Intracerebral
5.	P-05		20	Epidural	P-20		Subarachnoid
6.	P-01		21	Intracerebral	P-21		Intracerebral
7.	P-06		22	Intracerebral	P-22		Epidural
8.	P-07		23	Subarachnoid	P-23		Subdural
9.	P-08		24	Intracerebral	P-24		Intracerebral
10.	P-10		25	Subdural	P-25		Subarachnoid
11.	P-11		26	Subdural	P-26		Epidural
12.	P-12		27	Subdural	P-27		Subarachnoid
13.	P-13		28	Subdural	P-28		Epidural
14.	P-14		29	Subdural	P-29		Intracerebral
15.	P-15		30	Normal	P-30		Epidural

TABLE II

IMAGE OF BRAIN BLEEDING AND NORMAL BRAIN RESULT OF EDGE DETECTION WITH HYBRID THRESHOLDING METHOD

Patient Code	Stretching Results	Hybrid Thresholding Method	Patient Code	Stretching Results	Hybrid Thresholding Method
P-01			P-16		
P-02			P-17		
P-03			P-18		
P-04			P-19		
P-05			P-20		
P-01			P-21		
P-06			P-22		
P-07			P-23		
P-08			P-24		
P-10			P-25		
P-11			P-26		
P-12			P-27		
P-13			P-28		

Patient Code	Stretching Results	Hybrid Thresholding Method	Patient Code	Stretching Results	Hybrid Thresholding Method
P-14			P-29		
P-15			P-30		

The next step is to take the distinguishing feature of the previously represented shape or part using the PCA (Principal Component Analysis) method. The pixel value dataset is taken from one of the following images:

$$D = \begin{bmatrix} 0 & 0 & 0 & ... C_{10} \\ 0 & 128 & 128 & ... C_{20} \\ 0 & 0 & 255 & ... C_{30} \end{bmatrix} \quad (15)$$

Furthermore, Zero Means is carried out against the data above, first looking for the average vector from the dataset above. After obtaining the Zero Means matrix, the calculation is carried out to obtain the covariance matrix using the equation :

$$A = Y^T * Y \quad (16)$$

$$A = \begin{bmatrix} 0 & -85.3 & 85 & 0 & 0 & 0 \\ 0 & 42.7 & -85 & 85.3 & 42.7 & 42.7 \\ 0 & 42.7 & 170 & -85 & -85 & 170 \end{bmatrix}$$

$$A = \begin{bmatrix} 14501.09 & 3582.69 & -18092.31 \\ 3582.59 & 9048.29 & -1262.71 \\ -18092.31 & -1262.71 & 30732.29 \end{bmatrix}$$

Then look for the eigenvalues of the covariance matrix above with equation as follows:

$$[V, d] = eig (A) \quad (17)$$

Eigen vector

$$V = \begin{bmatrix} 592.051 & 355.198 & 517.933 \\ -66.130 & 474.322 & -144.332 \\ 412.475 & -16.851 & 439.493 \end{bmatrix}$$

Eigen value

$$V = \begin{bmatrix} 0.017 & 0 & 0 \\ 0 & 4.571 & 0 \\ 0 & 0 & 59.432 \end{bmatrix}$$

Then calculate the principal component analysis matrix with equation as follows:

$$PCA = (Y * v) \quad (18)$$

$$A = \begin{bmatrix} -697.204 & 878.845 & -906.523 & ... X_{10} \\ -883.531 & -859.180 & -818.151 & ... X_{20} \\ 767.531 & -724.378 & -693.507 & ... X_{30} \end{bmatrix} (19)$$
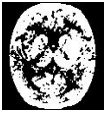
The test results using PCA are as follows table III :

TABLE III
THE TEST RESULTS USING PCA

PC1	PC2	PC3	PC4
-697.204	-878.845	-906.523	-883.438
859.180	-818.151	-767.530	-724.377
693.507	-643.226	-604.812	-581.139
544.745	-510.557	-435.835	-383.694
299.779	-239.896	-195.243	-169.753
144.332	-92.4123	-66.1305	-16.8509
3.678	78.21896	111.592	173.036
212.175	255.2500	332.167	355.198
366.711	329.2358	357.511	392.039
393.376	400.9839	474.321	520.571
550.412	540.0762	515.375	479.100
592.050	624.3587	636.336	643.461
658.560	637.0940	626.488	625.858
630.920	608.3942	581.798	578.338
561.301	517.9332	471.796	504.043
477.891	450.8046	457.077	458.573
504.209	476.8911	439.492	412.475
419.699	435.8440	406.652	347.216
305,364	316.8183	290.439	251.802
242.730	208.4953	164.327	92.236
32.7364	-45.7445	-96.9102	-194.417
297.468	-354.147	-411.592	-514.519
611.050	-661.003	-723.463	-782.844
846.225	-885.164	-904.616	-931.857
930.431	-752.278	-714.731	-708.555

Patient Code	Hybrid Thresholding Method	Area in Pixels (mm²)	Patient Code	Hybrid Thresholding Method	Area in Pixels (mm²)
P-01		0.00	P-16		0.00
P-02		0.00	P-17		0.00
P-03		2.530	P-18		1.764
P-04		2.336	P-19		3.037
P-05		3.085	P-20		2.101
P-01		3.001	P-21		6.911
P-06		1.594	P-22		5.810
P-07		3.033	P-23		5.629
P-08		3.369	P-24		5.840
P-10		3.791	P-25		6.839
P-11		9.102	P-26		8.268
P-12		2.606	P-27		6.339
P-13		2.661	P-28		1.845

Patient Code	Hybrid Thresholding Method	Area in Pixels (mm²)	Patient Code	Hybrid Thresholding Method	Area in Pixels (mm²)
P-14		3.00	P-29		1.681
P-15		9.117	P-30		2.181

In the final stage of testing, classifying brain hemorrhages through CT scan images is classified into 5 types of classification. From the results of the training carried out on a number of inputted data used as training data, the knowledge and information obtained from the training process will be used as a reference for classifying brain bleeding using the BNN.

In the BNN testing, a feed-forward direction is used, where in this phase, the data to be tested is the result of feature and pattern extraction and is not data from training. The weight generated from the training carried out is used as a reference value for calculating the output value at each node in the hidden layer. Furthermore, at the testing stage using the BNN method, external testing for each node in the outer layer. If the result of the node's output layer is > 0.1, then the output value of the node will be replaced with a value of 0. If the node's output layer is < 0.1, then the output value of the node will be changed to a value of 1. Where in the BNN testing process, the test data used for input is the weight of the training results.

The followings are the results of testing on 30 patients and the calculation of the area of brain bleeding using a mathematical morphology algorithm. The results of the extraction of the hybrid thresholding method can be seen in table V. It can be seen that 30 patients were tested, consisting of 4 normal without bleeding and 4 normal, 8 epidural strokes, 7 intracerebral strokes, 4 subarachnoid strokes and 7 subdural strokes. The results of the tests carried out resulted in 4 valid normal, 8 Epidural strokes, 2 differences, namely at P-30 and P-04 the Epidural should have changed P-30 to Subarachnoid stroke P-04 to Intracerebral stroke, 7 Intracerebral strokes were all valid, 4 Subarachnoid strokes valid and 7 Subdural strokes, there was a difference in P-13 which should have been a Subdural stroke turned into a Subarachnoid stroke as can be seen in table V.

TABLE V
IMAGE COMPARISON OF CALCULATION CLASSIFICATION RESULTS WITH DICOM TOOL AND USING HYBRID THRESHOLDING ANALYSIS (OTSU AND PCA) AND BAG ROGATION NEURAL NETWORK

No.	Patient Code	Pixel Bleeding Area Luas(mm²) with DICOM	Pixel Bleeding Area Luas(mm²) with System	Type (Stoke)	Results with Tools DICOM	System Testing Classification Result	Result of matching
1.	P-01	0.00	0.00	Normal	Normal	Normal	Valid
2.	P-02	0.00	0.00	Normal	Normal	Normal	Valid
3.	P-03	2.530	2.531	Medium	Epidural	Epidural	Valid
4.	P-04	2.336	4.336	heavy	Epidural	Intracerebral	Invalid
5.	P-05	3.085	3.085	heavy	Epidural	Epidural	Valid
6.	P-06	3.001	3.001	heavy	Intracerebral	Intracerebral	Valid
7.	P-07	1.594	1.594	Medium	Intracerebral	Intracerebral	Valid
8.	P-08	3.033	3.033	heavy	Subdural	Subdural	Valid
9.	P-09	3.369	3.369	heavy	Intracerebral	Intracerebral	Valid
10.	P-10	3.791	3.791	heavy	Subdural	Subdural	Valid
11.	P-11	9.102	9.102	heavy	Subdural	Subdural	Valid
12.	P-12	2.606	2.606	Medium	Subdural	Subdural	Valid
13.	P-13	2.661	5.661	heavy	Subdural	Subarachnoid	Invalid
14.	P-14	3.001	3.001	heavy	Subdural	Subdural	Valid
15.	P-15	9.117	9.117	heavy	Subarachnoid	Subarachnoid	Valid
16.	P-16	0.00	0.00	Normal	Normal	Normal	Valid
17.	P-17	0.00	0.00	Normal	Normal	Normal	Valid
18.	P-18	1.764	1.764	Medium	Intracerebral	Intracerebral	Valid
19.	P-19	3.037	3.037	heavy	Subarachnoid	Subarachnoid	Valid
20.	P-20	2.101	2.101	Medium	Intracerebral	Intracerebral	Valid
21.	P-21	6.911	6.911	heavy	Epidural	Epidural	Valid
22.	P-22	5.810	5.810	heavy	Subdural	Subdural	Valid
23.	P-23	5.629	5.629	heavy	Intracerebral	Intracerebral	Valid
24.	P-24	5.840	5.840	heavy	Subarachnoid	Subarachnoid	Valid
25.	P-25	6.839	6.839	heavy	Epidural	Epidural	Valid
26.	P-26	8.268	8.268	heavy	Subarachnoid	Subarachnoid	Valid
27.	P-27	6.339	6.339	heavy	Epidural	Epidural	Valid
28.	P-28	1.845	1.845	small	Intracerebral	Intracerebral	Valid
29.	P-29	1.681	1.681	small	Epidural	Epidural	Valid
30.	P-30	2.181	1.181	small	Epidural	Subarachnoid	Invalid

Based on the test data that has been carried out on the application of brain hemorrhage classification through CT Scan images using Hybrid Thresholding analysis (Otsu and PCA) and Backpropagation Neural Network, can be obtained accuracy values in identifying the area of brain bleeding and classification of stroke. From the calculation of the bleeding area, it can be seen that the level of accuracy of the method used in analyzing brain hemorrhage in classifying strokes with CT Scan images is 27/3 x 100% = 90.0%. Classification errors occur because of the similarity of features resulting from segmentation analysis and extraction using Hybrid Thresholding and classification with Backpropagation Neural Network. In this study, an error occurred in the classification of patients with patient codes P-04 from epidural to intracerebral stroke, P-13 from subdural to subarachnoid, and P-24 from epidural to subarachnoid. The results of calculating the number of white pixels after hybrid thresholding segmentation and feature extraction using PCA are similar.

IV. Conclusion

Tests that have been carried out to analyze and improve the image quality of brain bleeding stroke patients using HT produces very good image quality in analyzing the image of brain bleeding areas of stroke patients using the PCA method. Stroke patients. Then the classification using BNN was carried out from the results of segmentation and extraction of images of brain bleeding from stroke patients from the results of calculating the bleeding area. The test results show that the accuracy value is obtained in identifying the area of brain bleeding and stroke classification. The results of the calculation of the area of brain bleeding in stroke patients using the BNN method in analyzing brain bleeding stroke patients to classify CT scan images on brain bleeding stroke patients with an accuracy rate of 27/3 x 100% = 90.0%.

Classification errors occur because of the similarity of features resulting from segmentation analysis and extraction using Hybrid Thresholding and classification with Backpropagation Neural Network. The error is in the classification of patients with patient codes P-04 from epidural to intracerebral stroke, P-13 from subdural to subarachnoid, and P-24 from epidural to subarachnoid. The results of calculating the number of white pixels after hybrid thresholding segmentation and feature extraction using PCA are similar, resulting in an error in calculating the area.

References

[1] G. A. Roth, G. A. Mensah, C. O. Johnson, G. Addolorato, and E. Ammirati, "Global Burden of Cardiovascular Diseases and Risk Factors, 1990–2019: Update From the GBD 2019 Study," J. Am. Coll. Cardiol., vol. 76, no. 25, pp. 2982–3021, 2020, doi: 10.1016/j.jacc.2020.11.010.

[2] S. Virani et al., "Heart Disease and Stroke Statistics—2020 Update: A Report From the American Heart Association," Circulation, vol. 141, 2020, doi: 10.1161/CIR.0000000000000757.

[3] V. N. Jastal Udin Y, "Riset kesehatan dasar dalam angka Provinsi Sulawesi Tengah 2020." Badan Penelitian Dan Pengembangan Kesehatan Kementerian Kesehatan RI, Sulawesi Tengah, 2020. Nomor Katalog : 1102001.72, Nomor Publikasi : 72560.2002, ISSN / ISBN : 0215-2282, Tanggal Rilis : 2020-04-27. https://catalogue.nla.gov.au/Record/1481430%20

[4] W. Qiu et al., "Machine learning for detecting early infarction in acute stroke with non--contrast-enhanced CT," Radiology, vol. 294, no. 3, pp. 638–644, 2020.doi: 10.1148/radiol.2020191193.

[5] I. Rachmadanti, "Optimalisasi Faktor Eksposi Pada Protokol Head Computerized Tomography Scan (Head Ct-Scan) Untuk Memperoleh Resolusi Spasial Maksimal," Universitas Airlangga, 2020.

[6] M. Naganuma et al., "Alberta Stroke Program Early CT Score Calculation Using the Deep Learning-Based Brain Hemisphere Comparison Algorithm," J. Stroke Cerebrovasc. Dis., vol. 30, no. 7, p. 105791, 2021, doi: 10.1016/j.jstrokecerebrovasdis.2021.105791.

[7] S. Cai, F. Chai, C. Hu, X. Han, and S. Liu, "Research on nano-CT medical image processing based on embedded system," Microprocess. Microsyst., vol. 82, p. 103755, 2021, doi: 10.1016/j.micpro.2020.103755.

[8] P. Kambli, N. J. Santiago, and others, "Prediction Of Covid-19 Cases At The Early Stageusing Deep Learning Method Taken Over CT Scan Images," NVEO-Natural Volatiles & Essent. OILS Journal NVEO, pp. 5213–5236, 2021. Doi: https://doi.10.1109/ACCESS.2021.3105321.

[9] A. W. Jatmiko, "Efek Pemakaian Kontras Untuk Optimalisasi Citra Pada Pemeriksaan Diagnostik Magnetic Resonance Imaging (MRI)," J. Biosains Pascasarj., vol. 23, no. 1, pp. 28–39, 2021.

[10] S. Rani, B. K. Singh, D. Koundal, and V. A. Athavale, "Localization of Stroke Lesion in MRI Images Using Object Detection Techniques: A Comprehensive Review," Neurosci. Informatics, p. 100070, 2022, doi: 10.1016/j.neuri.2022.100070.

[11] G. Zhu, H. Chen, B. Jiang, F. Chen, Y. Xie, and M. Wintermark, "Application of Deep Learning to Ischemic and Hemorrhagic Stroke Computed Tomography and Magnetic Resonance Imaging," Semin. Ultrasound, CT MRI, vol. 43, no. 2, pp. 147–152, 2022, doi: 10.1053/j.sult.2022.02.004.

[12] T. Herrgårdh et al., "Hybrid modelling for stroke care: Review and suggestions of new approaches for risk assessment and simulation of scenarios," NeuroImage Clin., vol. 31, p. 102694, 2021, doi: 10.1016/j.nicl.2021.102694.

[13] Sumijan, P. Ayu Widya Purnama, and S. Arlis, "Multiple Thresholding Methods for Extracting & Measuring Human Brain and 3D Reconstruction," 2019, doi: 10.1088/1742-6596/1339/1/012027.

[14] M. J. Elizabeth, J. Jobin, and J. Dona, "A fog based security model for electronic medical records in the cloud database," Int. J. Innov. Technol. Explor. Eng., vol. 8, pp. 2552–2560, 2019.

[15] M. Irsal, N. Nurbaiti, A. N. Mukhtar, S. Gunawati, and W. Hidayat, "Effect of Tube Voltage on the Use of Iterative Reconstruction on Computed Tomography Brain Examination," J. Teor. dan Apl. Fis., vol. 9, no. 1, pp. 103–110, 2021. doi: 10.23960%2Fjtaf.v9i1.2715.

[16] I. K. G. D. Putra, D. Witarsyah, M. Saputra, and P. Jhonarendra, "Palmprint Recognition Based on Edge Detection Features and Convolutional Neural Network," Int. J. Adv. Sci. Eng. Inf. Technol., vol. 11, no. 1, pp. 380–387, 2021, doi: 10.18517/ijaseit.11.1.11664.

[17] T. R. Schneider et al., "Detection of intact Borrelia garinii in a sural nerve biopsy," Muscle \& Nerve, vol. 63, no. 6, pp. E52--E55, 2021.

[18] R. E. A. Armya and A. M. Abdulazeez, "Medical images segmentation based on unsupervised algorithms: a review," Qubahan Acad. J., vol. 1, no. 2, pp. 71–80, 2021. doi: doi.org/10.48161/qaj.v1n2a51.

[19] J. Manhas, R. K. Gupta, and P. P. Roy, "A Review on Automated Cancer Detection in Medical Images using Machine Learning and Deep Learning based Computational Techniques: Challenges and Opportunities," Arch. Comput. Methods Eng., pp. 1–41, 2021. doi:10.1007/s11831-021-09676-6.

[20] H. Zhu, L. Jiang, H. Zhang, L. Luo, Y. Chen, and Y. Chen, "An automatic machine learning approach for ischemic stroke onset time identification based on DWI and FLAIR imaging," NeuroImage Clin., vol. 31, p. 102744, 2021, doi: 10.1016/j.nicl.2021.102744.

[21] P. Kulkarni and Rajesh T. M., "A Multi-Model Framework for Grading of Human Emotion Using CNN and Computer Vision," Int. J. Comput. Vis. Image Process., vol. 12, no. 1, pp. 1–21, Jan. 2022, doi: 10.4018/IJCVIP.2022010102.

[22] A. Ramadhanu, J. Na'am, G. W. Nurcahyo, and - Yuhandri, "Development of Affine Transformation Method in the Reconstruction of Songket Motif," Int. J. Adv. Sci. Eng. Inf. Technol., vol. 12, no. 2, pp. 600–606, 2022, doi: 10.18517/ijaseit.12.2.16305.

[23] V. Feigin, M. Brainin, B. Norrving, S. Martins, R. Sacco, and Hacke, "World Stroke Organization (WSO): Global Stroke Fact Sheet 2022," Int. J. Stroke, vol. 17, pp. 18–29, 2022, doi: 10.1177/17474930211065917.

[24] J. K. Goswami, S. Jalal, C. S. Negi, and A. S. Jalal, "A Texture Features-Based Robust Facial Expression Recognition," Int. J. Comput. Vis. Image Process., vol. 12, no. 1, pp. 1–15, Jan. 2022, doi: 10.4018/IJCVIP.2022010103.

[25] J. Ramasamy, R. Doshi, and K. K. Hiran, "Segmentation of Brain Tumor using Deep Learning Methods: A Review," in Proceedings of the International Conference on Data Science, Machine Learning and Artificial Intelligence, 2021, pp. 209–215. doi: 10.1145/3484824.3484876.

[26] M. Platscher, J. Zopes, and C. Federau, "Image translation for medical image generation: Ischemic stroke lesion segmentation," Biomed. Signal Process. Control, vol. 72, p. 103283, 2022, doi: 10.1016/j.bspc.2021.103283.

[27] P. Modi and S. Patel, "A State-of-the-Art Survey on Face Recognition Methods," Int. J. Comput. Vis. Image Process., vol. 12, no. 1, pp. 1–19, Jan. 2022, doi: 10.4018/IJCVIP.2022010101.

[28] Y. Malkis and I. M. Kariasa, "Penerapan Teori Roy Dalam Meningkatkan Asuhan Keperawatan Pada Pasien Stroke Iskemia Berulang," J. Endur. Kaji. Ilm. Probl. Kesehat., vol. 7, no. 1, pp. 176–183, 2022. doi: 10.22216/endurance.v7i1.826.

[29] R. Rulaningtyas, K. Ain, and others, "CT scan image segmentation based on hounsfield unit values using Otsu thresholding method," in Journal of Physics: Conference Series, 2021, vol. 1816, no. 1, p. 12080. doi : 10.1088/1742-6596/1816/1/012080.

[30] F. Samopa and A. Asano, "Hybrid image thresholding method using edge detection," *Int. J. Comput. Sci. Netw. Secur.*, vol. 9, no. 4, pp. 292–299, 2009.

[31] N. Ohtsu, "An Automatic Threshold Selection Method Based on Discriminant and Least Squares Criteria," *Trans. IECE Japan, D*, vol. 63, no. 4, pp. 933–940, 2010. doi: 10.1109/CAR.2010.5456687.

[32] W.-S. Kim, S. Cho, D. Baek, H. Bang, and N.-J. Paik, "Upper extremity functional evaluation by Fugl-Meyer assessment scoring using depth-sensing camera in hemiplegic stroke patients," PLoS One, vol. 11, no. 7, p. e0158640, 2016. doi: 10.1371/journal.pone.0158640.

[33] Y. Shi, Z. Tian, M. Wang, Y. Wu, B. Yang, and F. Fu, "Residual convolutional neural network-based stroke classification with electrical impedance tomography," IEEE Trans. Instrum. Meas., 2022. doi: 10.1109/TIM.2022.3165786.

[34] L. M. Gottwald et al., "Pseudo-spiral sampling and compressed sensing reconstruction provides flexibility of temporal resolution in accelerated aortic 4D flow MRI: A comparison with k-t principal component analysis," NMR Biomed., vol. 33, no. 4, p. e4255, 2020. doi: 10.1002/nbm.4255.

[35] P. Bharath Kumar Chowdary, P. Jahnavi, S. S. Rani, T. J. Chowdary, and K. Srija, "Detection and Classification of Cerebral Hemorrhage Using Neural Networks," in Proceedings of Second International Conference on Advances in Computer Engineering and Communication Systems, 2022, pp. 555–564. doi: 10.1007/978-981-16-7389-4_54.

[36] R. Wang and H.-Y. Bi, "A predictive model for chinese children with developmental dyslexia—Based on a genetic algorithm optimized back-propagation neural network," Expert Syst. Appl., vol. 187, p. 115949, 2022. doi: 10.1016/j.eswa.2021.115949.

[37] C. Bie et al., "Motion correction of chemical exchange saturation transfer MRI series using robust principal component analysis (RPCA) and PCA," Quant. Imaging Med. Surg., vol. 9, no. 10, p. 1697, 2019. doi: 10.21037/qims.2019.09.14.

[38] A. Wadhwa, A. Bhardwaj, and V. S. Verma, "A review on brain tumor segmentation of MRI images," Magn. Reson. Imaging, vol. 61, pp. 247–259, 2019. doi: 10.1016/j.mri.2019.05.043.

[39] M. K. Abd-Ellah, A. I. Awad, A. A. M. Khalaf, and H. F. A. Hamed, "A review on brain tumor diagnosis from MRI images: Practical implications, key achievements, and lessons learned," Magn. Reson. Imaging, vol. 61, pp. 300–318, 2019. doi: 10.1016/j.mri.2019.05.028

[40] A. Jian, K. Jang, C. Russo, S. Liu, and A. Di Ieva, "Foundations of Multiparametric Brain Tumour Imaging Characterisation Using Machine Learning," in Machine Learning in Clinical Neuroscience, Springer, 2022, pp. 183–193. doi: 10.1007/978-3-030-85292-4_22.

[41] Ministry of Health of the Republic of Indonesia. Health Research and Development Agency. 2018 RISKESDAS National Report. Jakarta: Lembaga Penerbit Badan Penelitian dan Pengembagan Kesehatan; 2019.

[42] Yang, Y., Zuo, Z., Tam, F., Graham, S. J., Tao, R., Wang, N., & Bi, H. Y. (2019). Brain activation and functional connectivity during Chinese writing: An fMRI study. Journal of Neurolinguistics, 51, 199-211, doi: 10.1039/C8RA10142F.